JOURNAL OF PROPULSION AND POWER
Vol. 26, No. 5, September–October 2010

Numerical Analysis of Quasi-Steady-Combustion Characteristics in a Solid Rocket Motor

Sung Nam Lee* and Seung Wook Baek†
Korea Advanced Institute of Science and Technology, Daejeon 305-701, Republic of Korea
and
Kyung Moo Kim‡
Korea Agency for Defense Development, Daejeon 305-152, Republic of Korea

DOI: 10.2514/1.47520

A numerical code that simulates combustion phenomena occurring in a solid rocket motor is developed in this study using a preconditioning algorithm. A quasi-steady-combustion process was analyzed for a composite material in a submerged nozzle. The governing equations were solved using a dual-time stepping method combined with a finite volume method. The mass flux and pressure in the cell face were evaluated using the advective upwind splitting method scheme. The turbulence model uses a two-equation model combined with a turbulence closure model. The geometric conservation law is used to simulate transient propellant surface regression. The numerical results for solid rocket combustion were compared with experimental results with a composite propellant. The calculated pressure variation in the combustion chamber is in good agreement with the measured results.

Nomenclature

ai	=	NASA polynomial constant
Cp_o	=	heat capacity at constant pressure
D_k	=	diffusion coefficient
E	=	z flux vector
Ev	=	z viscous vector
F	=	r flux vector
Fv	=	r viscous vector
H	=	axisymmetric source term
h_i	=	enthalpy
P	=	pressure
Q	=	preconditioned primitive variable
q	=	heat flux
R	=	gas constant
r	=	radial direction distance
T	=	temperature
t	=	time
u	=	z velocity
V	=	velocity magnitude
V_{Free}	=	freestream velocity
v	=	r velocity
W	=	molecular weight
X	=	mole fraction
Y	=	mass fraction
z	=	axial direction distance
α	=	axisymmetric coefficient; 0 for a two-dimensional problem and 1 for an axisymmetric problem
Γ	=	preconditioning matrix
η	=	viscosity
κ	=	turbulent kinetic energy
λ	=	thermal conductivity
ρ	=	density
τ	=	total stress
υ	=	stoichiometric coefficients
Ωv	=	diffusion collision integral
ω	=	specific dissipation rate

Received 5 October 2009; revision received 27 January 2010; accepted for publication 10 March 2010.

*Ph.D. Candidate, Division of Aerospace Engineering, School of Mechanical, Aerospace & Systems Engineering, 373-1 Guseong-Dong, Yuseong.

†Professor, Division of Aerospace Engineering, School of Mechanical, Aerospace & Systems Engineering, 373-1 Guseong-Dong, Yuseong; swbaek@kaist.ac.kr.

‡Senior Researcher, Propulsion Department, Jochiwongil 462, Yuseong.

I. Introduction

FOR the past few decades, solid rocket motors have been extensively developed for tactical purposes and for civilian applications. Currently, many types of solid propellants are available and used for different purposes. However, the physical and chemical phenomena involved in a rocket combustion chamber are highly complex; hence, it remains difficult to predict realistically what occurs inside a solid rocket motor. Furthermore, experimental measurements and observations are other formidable tasks. Therefore, the development of a model that predicts the propellant regression as well as an understanding of the reacting flow inside the combustor would assist with the recognition of the interaction between the propellant surface regression and the rocket motor flow. This can lead to the better design of the nozzle and the grain configuration for specific missions. Thus far, many attempts have been made to comprehend solid rocket combustion. Beckstead et al. [1], Cazan and Menon [2], and McDonald and Menon [3] examined the reaction mechanism on the surface as well as in the gas phase with a composite propellant. Most previous research is limited to one-dimensional theory and simplified two-dimensional combustion. On the other hand, a more complex study [4] has dealt with complex numerical schemes. Examples include direct numerical simulation and the unstructured parallel code, which requires a significant increase in the computational time. For example, the Center for the Simulation of Advanced Rockets (CSAR) at the University of Illinois at Urbana–Champaign has been studying solid propellant rockets to predict the physical characteristics of entire systems from fluids to materials with computational fluid dynamics (CFD). CSAR reported results for ammonium-perchlorate/hydroxyl-terminated-polybutadiene (AP/HTPB) propellant combustion with and without aluminized particles. In the present study, however, the objective is to simulate the combustion characteristics in a solid rocket motor together with the propellant surface regression phenomenon using a simple numerical scheme requiring only a moderate amount of computational time.

Consequently, in this paper, composite propellant combustion with a submerged nozzle is numerically investigated with structured

multiblocks. The results are compared with available experimentally measured data. The development of a reacting flow in the gas phase and the surface regression are unsteadily simulated using a moving grid with the geometric conservation law (GCL) [5]. The transient grain variation is also traced in this work. Finally, the transient thrust variation is calculated. The physical phenomena occurring inside a solid rocket motor comprise two different physical domains. The first is a subsonic area inside the combustor, in which the solid propellant regresses, and in the converging nozzle section. The second is a supersonic regime inside the diverging nozzle section. Therefore, neither a compressible algorithm based on density nor an incompressible method such as SIMPLE is suitable for simulating the performance of a solid rocket motor. Therefore, to investigate the reacting flow in a solid rocket motor reliably, the preconditioning algorithm by Weiss and Smith [6] and Shuen et al. [7] is adopted here. This preconditioning technique provides stability in solving the problem at various speed ranges.

II. Computational Method

A schematic of the solid rocket examined in this work is illustrated in Fig. 1a. The propellant grain is shown in Fig. 1b, the nozzle of a submerged shape is shown in Figs. 1a and 1b, and the ground test apparatus is shown in Fig. 1c. The propellants used here include 4 kg of HTPB, AP, and Al. The grain length is 0.264 m and the web thickness is 0.025 m.

The surface burning rate is defined in Eq. (1). The observed burning rate was approximately 11.1 mm/s when $a = 0.02293$ and $n = 0.4321$.

$$r_b = a p^n \tag{1}$$

The nozzle throat diameter is 0.025 m and the expansion ratio is 7.84. The grain shape is a type of internal burning tube. The averaged pressure and thrust are 56 atm and 4.3 kN, and these are compared with the numerical data. The burning time is approximately 2.25 s when the temperature coefficient is 0.023 and the burning rate exponent is 0.43.

The governing equations include the Navier–Stokes, energy, species, and turbulence equations for the gas phase and a heat conduction equation for the solid propellant. The gas-phase equation for a 2-D axisymmetric flow is cast in the following form following Weiss and Smith [6] and Shuen et al. [7]:

$$\Gamma \frac{\partial Q}{\partial t} + \frac{\partial (E - E_V)}{\partial z} + \frac{\partial (F - F_V)}{\partial r} = \alpha H \tag{2}$$

Here, Γ represents the preconditioning matrix that controls the eigenvalues, E and F are flux terms, and E_v and F_v are diffusive terms. H is an axisymmetric term; α is 0 for a two-dimensional problem and 1 for an axisymmetric problem.

$$\Gamma = \begin{pmatrix} \rho_p & 0 & 0 & \rho_T & 0 & 0 & 0 & & \\ \rho_p u & \rho & 0 & \rho_T u & 0 & 0 & 0 & & \\ \rho_p v & 0 & \rho & \rho_T v & 0 & 0 & 0 & & \\ & \rho_p H - 1 & \rho u & \rho v & & \rho_T H + \rho c_p & 0 & 0 & 0 \\ & \rho_p \kappa & 0 & 0 & & \rho_T \kappa & \rho & 0 & 0 \\ & \rho_p \omega & 0 & 0 & & \rho_T \omega & 0 & \rho & 0 \\ & \rho_p Y_i & 0 & 0 & & \rho_T Y_i & 0 & 0 & \rho \end{pmatrix}$$

$$\rho_p = \frac{1}{U_{\text{ref}}} + \frac{1}{C_p T}$$

$$\rho_T = -\frac{\rho}{T}$$

$$U_{\text{ref}} = \min(a, \max(V, 0.5 V_{\text{free}}))^2$$

$$Q = [p, u, v, T]^T, [\kappa, \omega]^T, [Y_i]^T$$

$$E = [\rho u, \rho u^2 + \rho, \rho uv, \rho uH, \rho u\kappa, \rho u\omega]^T$$

$$F = [\rho v, \rho uv, \rho v^2 + p, \rho vH, \rho v\kappa, \rho v\omega]^T$$

$$E_v = [0, \tau_{zz}, \tau_{zr}, u\tau_{zz} + v\tau_{zr} + q_z, \tau_{\kappa z}, \tau_{\omega z}]^T$$

$$F_v = [0, \tau_{zr}, \tau_{rr}, u\tau_{zr} + v\tau_{rr} + q_r, \tau_{\kappa r}, \tau_{\omega r}]^T$$

The total enthalpy is

$$H = \sum_{i=1}^{\text{Ns}} Y_i h_i + \frac{1}{2}(u^2 + v^2) \tag{3}$$

To acquire the solution, the inverse of matrix Γ must be calculated. However, the matrix inversion becomes highly complicated as the number of species increases. Therefore, a semi-implicit method is applied to overcome this problem [8]. To predict the surface regression phenomena, the GCL scheme [5] is applied to the preconditioned Navier–Stokes equation. When Ω is the control volume, v_{gn} is the grid velocity, and S_f is the cell face area, the change of volume is equivalent to the cell face movement rate such that

$$\frac{\Omega^{n+1} - \Omega^n}{dt} = \sum_f v_{gn} dS_f \tag{4}$$

Consequently, using Eq. (1), Eq. (4) is modified as follows:

$$\Gamma \frac{Q^{n+1}\Omega^{n+1} - Q^n \Omega^n}{dt} + \sum_f (E - E_v - Qu_g) dS_f + \sum_f (F - F_v - Qv_g) dS_f = \alpha H \Omega \tag{5}$$

A. Inviscid Flux

A modified advective upwind splitting method (AUSM$^+$ − up) [9] is used to deal with the flux term in the Navier–Stokes equation. The AUSM method was developed to overcome the defect of the Roe scheme, that is, slow convergence at a low speed. Liou [9] proposed that the AUSM$^+$ − up method can be used in any range from a subsonic flow to a supersonic flow. When applying the AUSM$^+$ − up method to the inviscid flux terms in Eq. (1), they become

$$E, F = \dot{m}_{1/2} \begin{cases} \boldsymbol{\phi}_L \\ \boldsymbol{\phi}_R \end{cases} + P_{1/2} \tag{6}$$

$$M_{1/2} = \mu^+_{(4)}(M_L) + \mu^-_{(4)}(M_R) - \frac{K_P}{f_a} \max(1 - \sigma \bar{M}^2, 0) \frac{P_R - P_L}{\rho_{1/2} a^2_{1/2}}$$

$$P_{1/2} = P^+_{(5)}(M_L) P_L + P^-_{(5)}(M_R) P_R - K_u P^+_{(5)} P^-_{(5)} (\rho_L + \rho_R) f_a a_{1/2} (u_R - u_L) \tag{7}$$

$$\dot{m}_{1/2} = a_{1/2} M_{1/2} \begin{cases} \rho_L \\ \rho_R \end{cases} \tag{8}$$

$$\boldsymbol{\phi} = \begin{pmatrix} 1 \\ u \\ v \\ H \end{pmatrix} \tag{9}$$

B. Shear Stress Transport Model

To account for turbulence behavior, shear stress turbulence modeling [10] is used. The two-equation model is based on a low Reynolds number; thus, the compressibility factor in the supersonic region must be corrected.

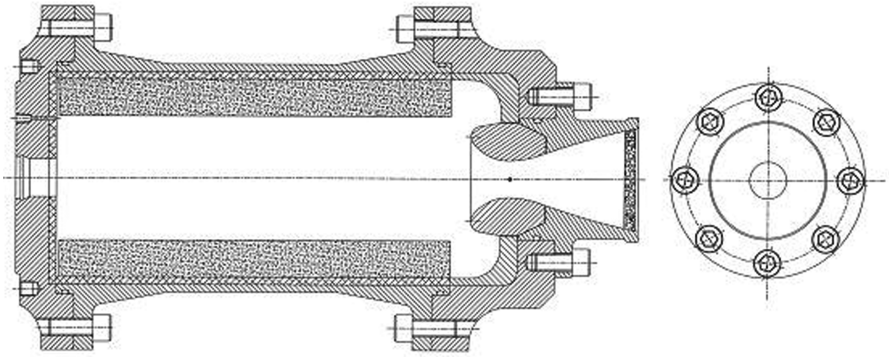

a) Test motor with a submerged nozzle

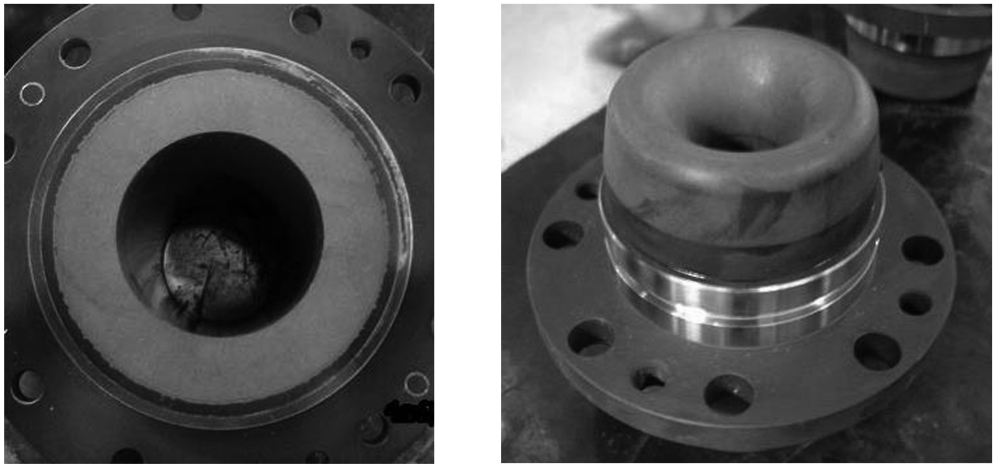

b) Solid rocket motor (left: charged propellant, right: nozzle assembly)

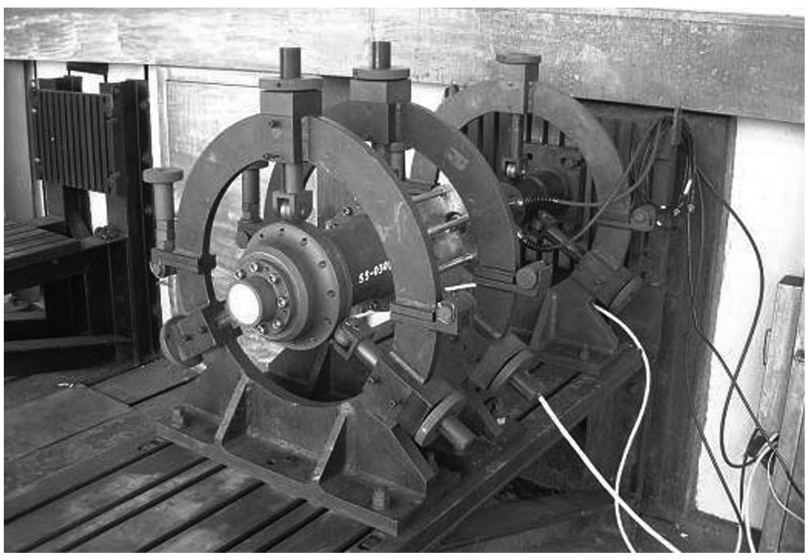

c) Ground test apparatus

Fig. 1 Schematic of an experimental rocket motor.

The equations for the turbulent kinetic energy and specific dissipation rate in this problem are written as follows:

$$\frac{\mathrm{D}(\rho k)}{\mathrm{D}t} = \tau_{ij}\frac{\partial u_i}{\partial x_j} - \beta^*\rho\omega\kappa + \frac{\partial}{\partial x_j}\left[(\mu + \sigma_k\mu_t)\frac{\partial k}{\partial x_j}\right] \tag{10}$$

$$\frac{\mathrm{D}(\rho\omega)}{\mathrm{D}t} = \frac{\gamma}{\nu_t}\tau_{ij}\frac{\partial u_i}{\partial x_j} - \beta\rho\omega^2 + \frac{\partial}{\partial x_j}\left[(\mu + \sigma_\omega\mu_t)\frac{\partial \omega}{\partial x_j}\right] + 2\rho(1 - F_1)\sigma_{\omega_2}\frac{1}{\omega}\frac{\partial \kappa}{\partial x_j}\frac{\partial \omega}{\partial x_j} \tag{11}$$

The eddy viscosity can be written as follows:

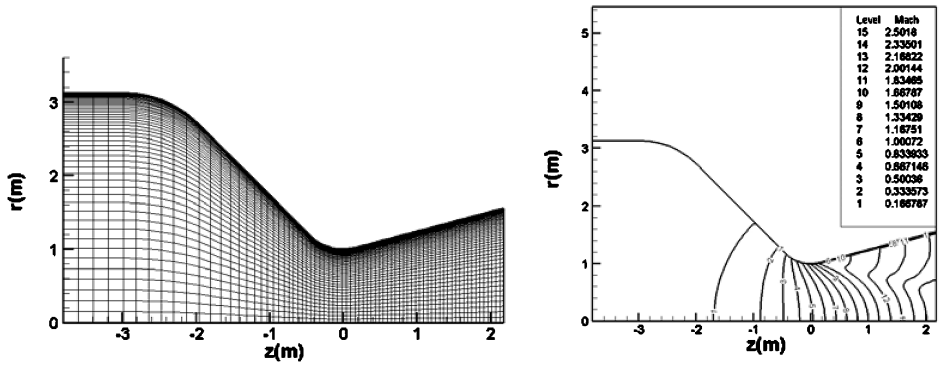

a) Grid generation (70×40) **b) Mach contour**

Fig. 2 Grid and Mach contour for a JPL nozzle.

$$\mu_t = 0.31\rho k/\mathrm{MAX}(0.31\omega, \Omega F_2)$$

$$\Omega = \left|\frac{\partial u}{\partial y} - \frac{\partial v}{\partial x}\right|, \qquad F_2 = \tanh(\arg_2^2),$$

$$\arg_2^2 = \mathrm{MAX}\left(2\frac{\sqrt{k}}{0.09\omega y}, \frac{500v}{y^2\omega}\right)$$

C. Chemical Kinetic Model

There are too many species generated from the solid propellant combustion to consider all of them. Moreover, the reaction mechanisms in the propellant surface and the gas phase are so complex that it is a formidable problem to establish all the chemical kinetics involved. Consequently, in this study a simplified chemical mechanism is applied to predict the combustion characteristics inside a rocket motor.

A composite propellant is considered here. This composite propellant comprises AP and an HTPB binder. The chemical compositions of AP and HTPB are NH_4ClO_4 and $C_{72.307}H_{110.389}O_{1.265}$. The composite propellant is distributed randomly in contrast to a double-base propellant, making it much harder to estimate the gas-phase chemical kinetics. In this study, four species are selected to represent the reacting flow involved: AP, APd (AP decomposition), binder, and product gas [2]. The reaction scheme applied here is as follows:

$$\mathrm{AP} \rightarrow \mathrm{APd} \tag{12}$$

$$R_1 = 2.234 \times 10^7 P(\mathrm{atm})[\mathrm{AP}]\exp(-E_1/R_uT)$$
$$\beta\mathrm{APd} + \mathrm{binder_{gas}} \rightarrow \text{combustion products} \tag{13}$$

$$R_2 = 1.105 \times 10^7 P(\mathrm{atm})[\mathrm{APd}][\mathrm{binder_{gas}}]\exp(-E_2/R_uT)$$

The activation temperatures for reactions 1 and 2 are $E_1/R_u = 8000$ K and $E_2/R_u = 11,000$ K, respectively.

D. Thermodynamic and Transport Properties

The temperature-dependent enthalpy and specific heat used here are as follows:

$$h_i = h_{fi}^o + \int_{T_{\mathrm{ref}}}^{T} Cp_i\,\mathrm{d}T \tag{14}$$

$$Cp_i = 1800 \tag{15}$$

Here, h_i and C_{pi} represent the enthalpy and specific heat, respectively, for species I [3].

The transport properties, thermal conductivity, and viscosity are calculated using the following relationships [2]:

$$D_k = \eta/Pr/\rho, \qquad \eta = 8.7 \times 10^{-8}\sqrt{W_k}T^{0.65},$$
$$\lambda = 1.08 \times 10^{-4}T + 0.0133 \tag{16}$$

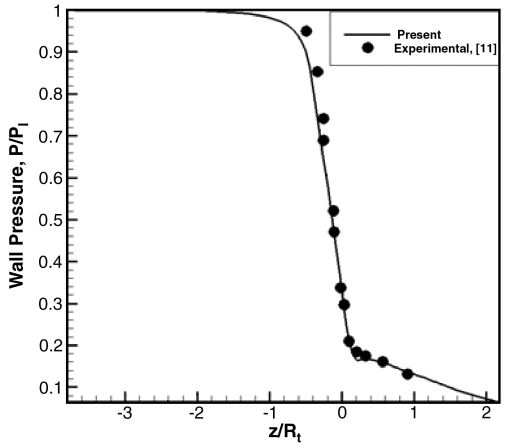

a) Wall pressure

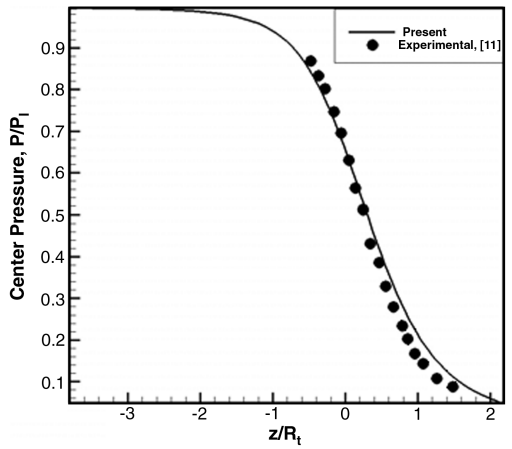

b) Center pressure

Fig. 3 Comparison of pressure variation.

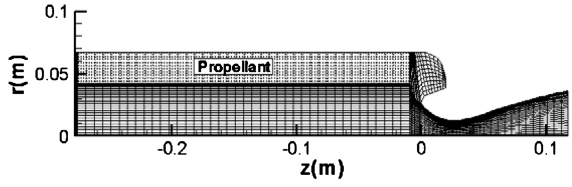

Fig. 4 Multiblock grid.

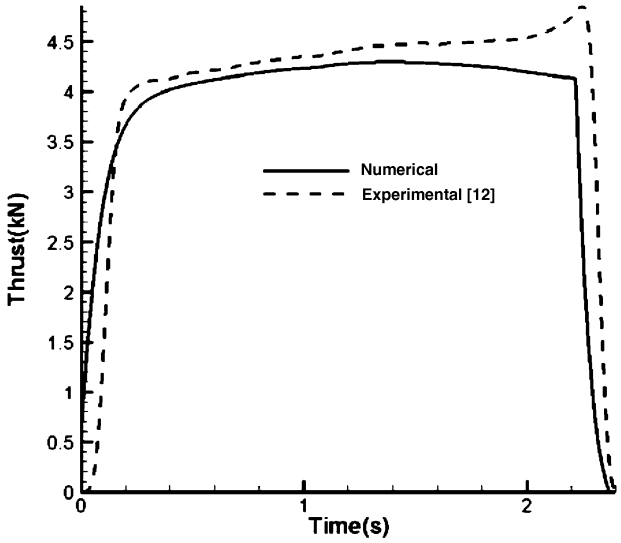

a) Thrust variation

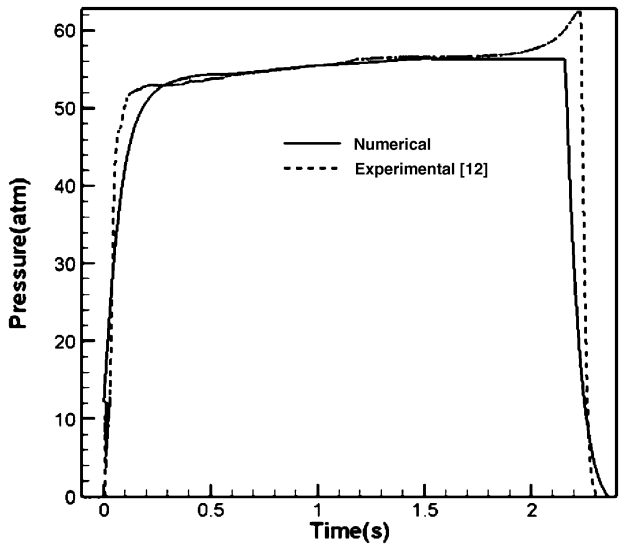

b) Pressure variation

Fig. 5 Comparison of the numerical and experimental results.

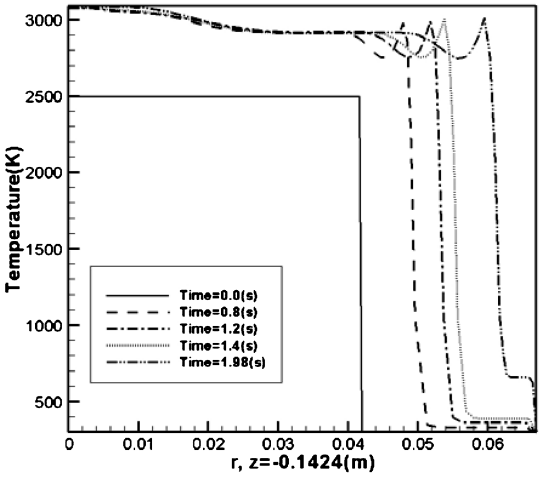

Fig. 6 Temperature profile along the radial direction at $z = -0.1424$ m.

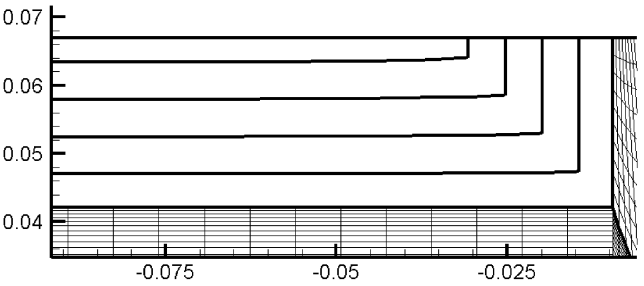

Fig. 7 Propellant surface at various time steps (0.02, 0.5, 1.0, 1.5, and 2.0 s).

E. Boundary Condition

The walls have a no-slip boundary condition.
At the symmetric line

$$\frac{\partial p}{\partial y} = 0, \qquad \frac{\partial T}{\partial y} = 0, \qquad \frac{\partial u}{\partial y} = 0, \qquad v = 0 \tag{17}$$

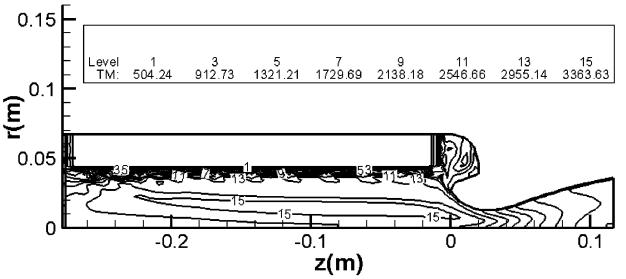

a) 0.02s

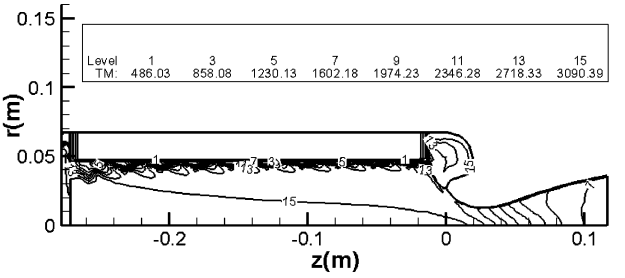

b) 0.5s

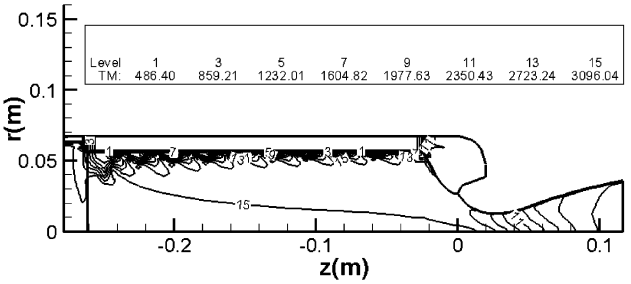

c) 1.5s

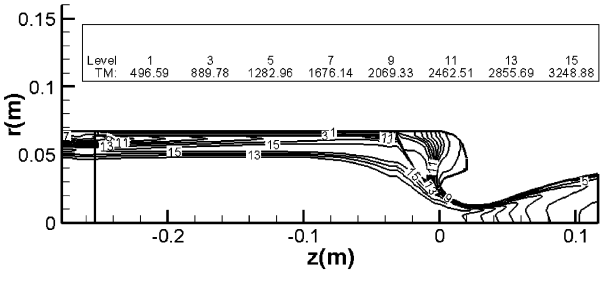

d) 2.2s

Fig. 8 Transient variation of the temperature contour.

Solid propellant surfaces

$$\frac{\partial p}{\partial y} = 0.5\rho\frac{\partial v^2}{\partial y}, \qquad u = 0, \qquad v = \rho_s r_b/\rho_g \tag{18}$$

$$(\rho v Y_i) - \rho_s r_b Y_{i,s} - \left(\rho D\frac{\partial Y_i}{\partial y}\right) = 0 \quad \text{where } Y_{\text{AP}} = 1$$
$$\text{else } Y_i = 0 \text{ at the AP area,} \tag{19}$$
$$Y_{\text{HTPB}} = 1 \quad \text{else } Y_i = 0 \text{ at the binder area}$$

$$\lambda_g\frac{\partial T}{\partial r} = (T_s - T_{si})\rho_s c_s r_b + \rho_s r_b[(c_p - c_s)\times(T_s - T_{s,\text{ref}}) + Q_{s,\text{ref}}] \tag{20}$$

$$\rho_s = 1800 \text{ kg/m}^3, \qquad c_s = 1256 \text{ J/kg}\cdot\text{K}$$
$$Q_s = 11.6\times 10^5 \text{ J/kg[2]}$$

F. Solid Conduction Equation

$$\rho_c C_c\frac{\partial T}{\partial t} = \lambda_c\frac{\partial^2 T}{\partial x^2} + \lambda_c\frac{\partial^2 T}{\partial y^2} \tag{21}$$

III. Numerical Simulation

A. Numerical Validation

To validate the computational code developed here, a Jet Propulsion Laboratory, California Institute of Technology (JPL) nozzle flow is calculated. Figure 2 shows the computational grid used and the resulting Mach contour. The numerical values of the pressure variation are compared with the experimental value from Cuffel et al. [11] in Fig. 3. As shown in the figure, they are in good agreement.

B. Numerical Results

Figure 4 illustrates the grid generation used in this study. It consists of four multiblocks with 2870 meshes. The chamber pressure and temperature were initially set to 10 atm and 2500 K, respectively, up at the nozzle throat to ignite the solid propellant. Consequently, this study does not exactly simulate the ignition transient phenomenon. Once the solid propellant in the combustor is ignited, it regresses

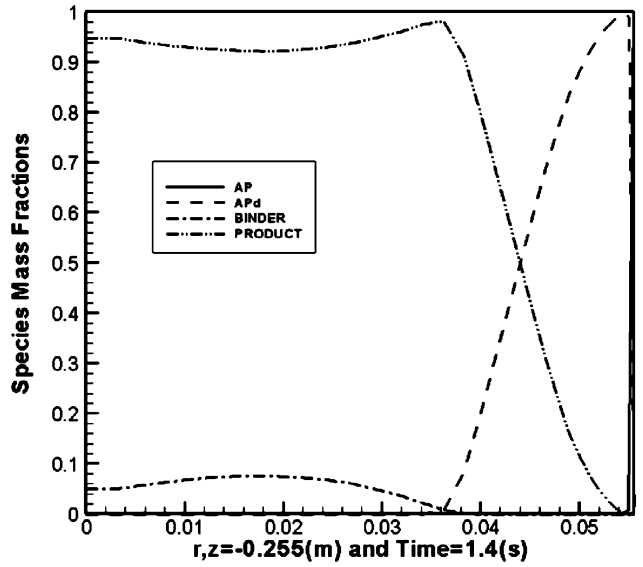

a) z=-0.255m at t=1.4 s

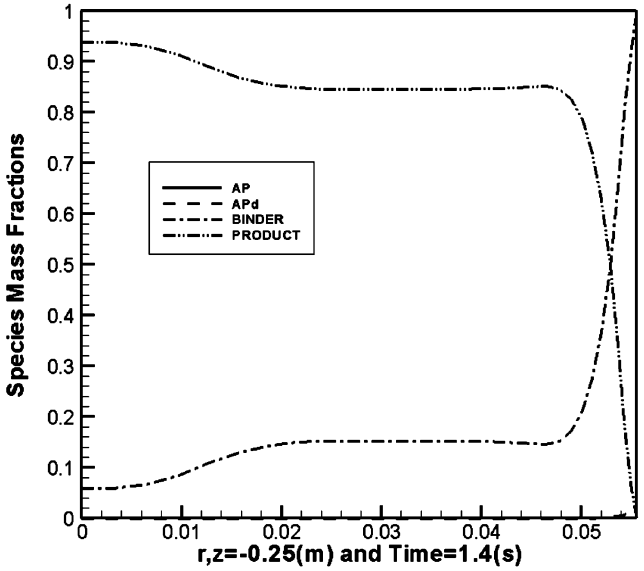

b) z=-0.25m at t=1.4 s

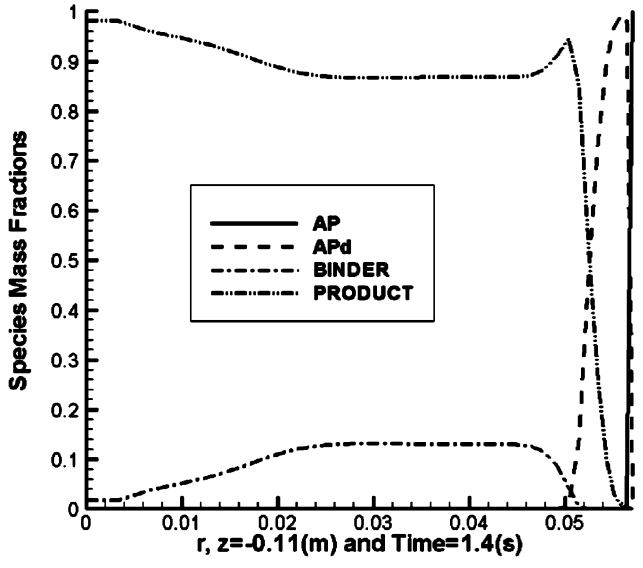

c) z=-0.13m at t=1.4 s

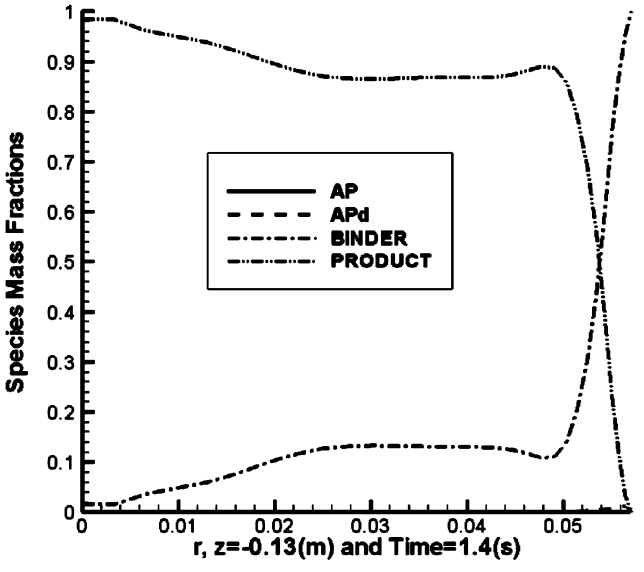

d) z=-0.11m at t=1.4 s

Fig. 9 Species mass fractions along the radial direction at different axial locations.

temporally. To simulate the combustion behavior of a rocket motor, the grid representing the propellant area is regenerated as time increases. The regression distance of the grid due to the burning propellant is determined by a time step and by the propellant burning rate:

$$\mathrm{d}\, z_{\mathrm{grid}} = \mathrm{d}t \times r_b$$

The propellant examined here is composed of AP/HTPB. The thrust and pressure variations are compared with the experimental data [12] in Fig. 5. Although the numerical results for the thrust are less than the experimental values, the pressure variation either is close to agreement with the data or predicts slightly smaller values. Because of the lower pressure overall, the numerical data for thrust become slightly lower than the experimental value.

According to the rocket configuration in Fig. 4, the radial temperature distribution from the axis of symmetry to the rocket wall is plotted at the axial location of $z = -0.1424$ m in Fig. 6. As time passes, the propellant surface is observed to shift toward the right side. The high-temperature region represents the gas phase, which is full of product gases. The temperature is observed to decrease rapidly in the solid propellant.

In the experiments, the measured burning rate for the composite propellant was approximately 0.011 m/s and the initial thickness of the propellant was 0.025 m. After the ignition of the propellant, the propellant burnout time was observed to be nearly 2.25 s. As an experimental observation of surface regression is arduous, the grain surface regression is numerically calculated. This is plotted in Fig. 7. The grain surface was found to decrease continually at a rate of 0.011 m/s. A depiction of the transient variation of the temperature contour is shown in Fig. 8. Because of the heterogeneous packing of the composite propellants, the temperature contours are shown to be irregular over the propellant surface. Figure 9 shows the species profiles along the radial direction at $z = -0.255$, -0.25, -0.13, and -0.11 m for a time of 1.4 s. The composite propellant used in this study is composed of 25% HTPB and 75% AP by volume. To model this type of composite propellant, one grid of equal space is assigned to HTPB, and three grids are assigned to AP so that a regular distribution over the propellant surface can be assumed. As a result, the HTPB mass fraction is 1 on one grid point of HTPB, and the AP mass fraction is 1 on the next three grid points, with this pattern continuing. Regarding the chemical reaction based on this type of composite propellant shown in Fig. 9, the reaction is not complete over the AP burning surface until the binder gas diffuses toward the gas region of APd, which is a type of diffusion-controlled flame. On the other hand, the binder gas directly changes to a product gas over the binder burning surface, which is a type of premixed flame. Furthermore, the reaction becomes more active along the downstream due to the increased axial velocity, which finally leads to an erosive burning effect. The location of -0.255 belongs to the AP section, and the -0.25 location belongs to the binder region. This explains why the corresponding species profile is so different. In Figs. 9c and 9d, the location of -0.11 belongs to the AP section, and the -0.13 location belongs to the binder region. Similar trends are observed depending on the location of the AP and binder.

These species profiles are closely related to the irregular temperature variation near the propellant surface in Fig. 8. A comparison of the temperature profile at 1.4 s in Fig. 6 with the species profiles at 1.4 s in Fig. 9 illustrates that the zone in which the gas temperature increases rapidly corresponds to the region in which the binder gas decreases rapidly and the product gas increases.

Gas acceleration along a convergent and divergent nozzle is confirmed by the continual decrease in the gas temperature therein.

IV. Conclusions

In this study, a computational code was developed to simulate the combustion characteristics of a solid rocket motor. A composite as well as a double-base propellant were considered. To predict the propellant regression characteristics, the moving grid scheme was adopted, and together with GCL technique, this produced very accurate results. The transient chamber pressure and thrust in the numerical solution with the composite propellant were compared with available experimental data. The pressure variation and thrust were validated by controlling the enthalpy of the formation of the propellants. Based upon the findings, the numerical algorithm adopted here was found to successfully simulate the subsonic combustion phenomena in a solid rocket motor, the subsonic flow in a convergent nozzle, and the supersonic flow in a divergent nozzle.

Acknowledgment

This work was supported by the Korea Science and Engineering Foundation grant 2010-0000353, funded by the Ministry of Education, Science & Technology.

References

[1] Beckstead, M. W., Derr, R. L., and Price, C. F., "A Model of Composite Solid-Propellant Combustion Based on Multiple Flames," *AIAA Journal*, Vol. 8, No. 12, 1970, pp. 2200–2207. doi:10.2514/3.6087

[2] Cazan, R., and Menon, S., "Direct Numerical Simulation of Sandwich and Random-Packed Propellant Combustion," AIAA Paper 2003-5082, 2003.

[3] McDonald, B. A., and Menon, S., "Direct Numerical Simulation of Solid Propellant Combustion in Crossflow," *Journal of Propulsion and Power*, Vol. 21, No. 3, 2005, pp. 460–469. doi:10.2514/1.10049

[4] "CSAR Annual Report," Center for the Simulation of Advanced Rockets, University of Illinois at Urbana–Champaign, Urbana, IL, 2004–2006.

[5] Thomas, P. D., and Lombard, C. K., "Geometric Conservation Law and Its Application to Flow Computations on Moving Grids," *AIAA Journal*, Vol. 17, No. 10, 1979, pp. 1030–1037. doi:10.2514/3.61273

[6] Weiss, J. M., and Smith, W. A., "Preconditioning Applied to Variable and Constant Density Flows," *AIAA Journal*, Vol. 33, No. 11, 1995, pp. 2050-2057. doi:10.2514/3.12946

[7] Shuen, J.-S., Chen, K.-H., and Choi, Y., "A Coupled Implicit Method for Chemical Non-Equilibrium Flows at All Speeds," *Journal of Computational Physics*, Vol. 106, No. 2, June 1993, pp. 306–318.

[8] Chen, K. H., Fricker, D., Lee, J., and Moder, J., "ALLSPD-3D User Guide," Ver. 2.0a., NASA Lewis Research Center, Turbomachinery and Propulsion Systems Division, 1998,

[9] Liou, M. S., "A Sequel to AUSM, Part II: AUSM$^+$ − up for All Speeds," *Journal of Computational Physics*, Vol. 214, 2006, pp. 137–170. doi:10.1016/j.jcp.2005.09.020

[10] Garg, V. K., and Ameri, A. A., "Two-Equation Turbulence Models for Prediction of Heat Transfer on a Transonic Turbine Blade," NASA CR 2001-210810, 2001.

[11] Cuffel, R. F., Back, L. H., and Massier, P. F., "Transonic Flowfield in a Supersonic Nozzle with Small Throat Radius of Curvature," *AIAA Journal*, Vol. 7, No. 7, 1969, pp. 1364–1366. doi:10.2514/3.5349

[12] Kim, K. M., "Interim Report in ADD," Korean Agency for Defense Development, Rept. ADDR S416-08121, 2008.

S. Son
Associate Editor